nature nanotechnology

LETTERS

PUBLISHED ONLINE: 17 NOVEMBER 2013 | DOI: 10.1038/NNANO.2013.241

Spin Hall effect clocking of nanomagnetic logic without a magnetic field

Debanjan Bhowmik†, Long You† and Sayeef Salahuddin*

Spin-based computing schemes could enable new functionalities beyond those of charge-based approaches[1–6]. Examples include nanomagnetic logic, where information can be processed using dipole coupled nanomagnets[7–14], as demonstrated by multi-bit computing gates[8,13]. One fundamental benefit of using magnets is the possibility of a significant reduction in the energy per bit compared with conventional transistors[1,8,14,15]. However, so far, practical implementations of nanomagnetic logic have been limited by the necessity to apply a magnetic field for clocking[8,11]. Although the energy associated with magnetic switching itself could be very small, the energy necessary to generate the magnetic field renders the overall logic scheme uncompetitive when compared with complementary metal–oxide–semiconductor (CMOS) counterparts. Here, we demonstrate a nanomagnetic logic scheme at room temperature where the necessity for using a magnetic field clock can be completely removed by using spin–orbit torques[16–22]. We construct a chain of three perpendicularly polarized CoFeB nanomagnets on top of a tantalum wire and show that an unpolarized current flowing through the wire can 'clock' the perpendicular magnetization to a metastable state. An input magnet can then drive the nanomagnetic chain deterministically to one of two dipole-coupled states, '2 up 1 down' or '2 down 1 up', depending on its own polarization. Thus, information can flow along the chain, dictated by the input magnet and clocked solely by a charge current in tantalum, without any magnetic field. A three to four order of magnitude reduction in energy dissipation is expected for our scheme when compared with state-of-the-art nanomagnetic logic.

The underlying physics of the clocking hinges on the recent demonstration that magnetization of a thin ferromagnet can be effectively controlled by charge current flowing in a heavy metal sitting immediately under the magnet[16–22]. Essentially, a current-induced spin-orbit torque controls the magnetization, although the exact nature of the torque is still being debated[18,22]. The heterostructure (Ta/CoFeB/MgO/Ta from the bottom) used here closely resembles that described in the work of Liu and colleagues[16], so, following their convention, we shall henceforth refer to the phenomenon as the spin Hall effect. Within spin Hall physics, when an in-plane current flows through a resistive bar made of ß-phase tantalum, electrons with spins of opposite polarities accumulate at the opposite surfaces along the thickness of the bar[16,17,23] (Fig. 1a) and could exert a torque on a magnet (CoFeB) sitting immediately on top of the tantalum. The CoFeB, in this case, has perpendicular magnetic anisotropy[24]. The in-plane torque, if strong enough, can bring its magnetization in-plane, where it is metastable. This is reflected in a reduction in coercivity to zero[25] (Supplementary Section 1). If the current is now turned off, the magnet, from this metastable state, will randomly go to an 'up' or 'down' state, determined by thermal noise. The ability to drive the magnet to a metastable state allows one to use it as an efficient clocking mechanism. For example, let us imagine a situation where there is a chain of three nanomagnetic dots located on top of a tantalum bar. Application of a current pulse (clock) through the tantalum would drive the magnets in-plane (Fig. 1b). On removal of the current, the magnets would orient themselves in their lowest energy configuration, 2 up 1 down (↑↓↑) or 2 down 1 up (↓↑↓),

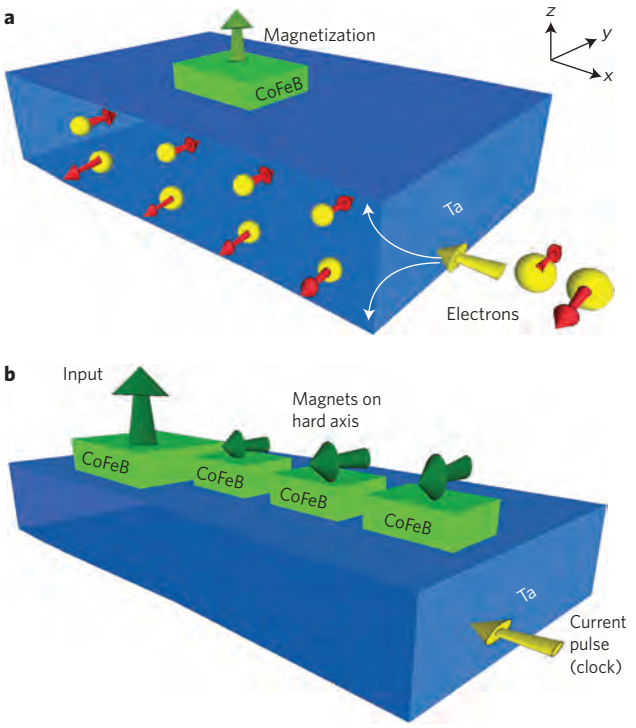

Figure 1 | Spin Hall effect spin-torque-based clocking. a, In-plane current flowing through tantalum along the *x*-direction (electrons along the −*x*-direction) causes spin separation across the thickness of the tantalum (*z*-direction). This results in accumulation of electrons with *y*-directed spins at the Ta/CoFeB interface, which offers spin Hall effect spin torque to the magnetization (green arrow) of CoFeB. This spin torque drives the magnetization of CoFeB from its easy axis in the out-of-plane direction to a metastable in-plane state. **b**, When current passes through the tantalum bar below the magnetic dots, magnetizations of all dots other than the large input dot are driven in-plane to a metastable state. Current flows in the −*x*-direction here, so electrons with −*y*-directed spins accumulate at the Ta/CoFeB interface, resulting in the magnetizations of the dots being driven to the −*y*-direction. When the current pulse is removed, the magnets go to the dipole-coupled lowest-energy configuration.

Department of Electrical Engineering and Computer Sciences, UC Berkeley, 253 Cory Hall, Berkeley, California 94720-1770, USA, †These authors contributed equally to this work. *e-mail: sayeef@eecs.berkeley.edu

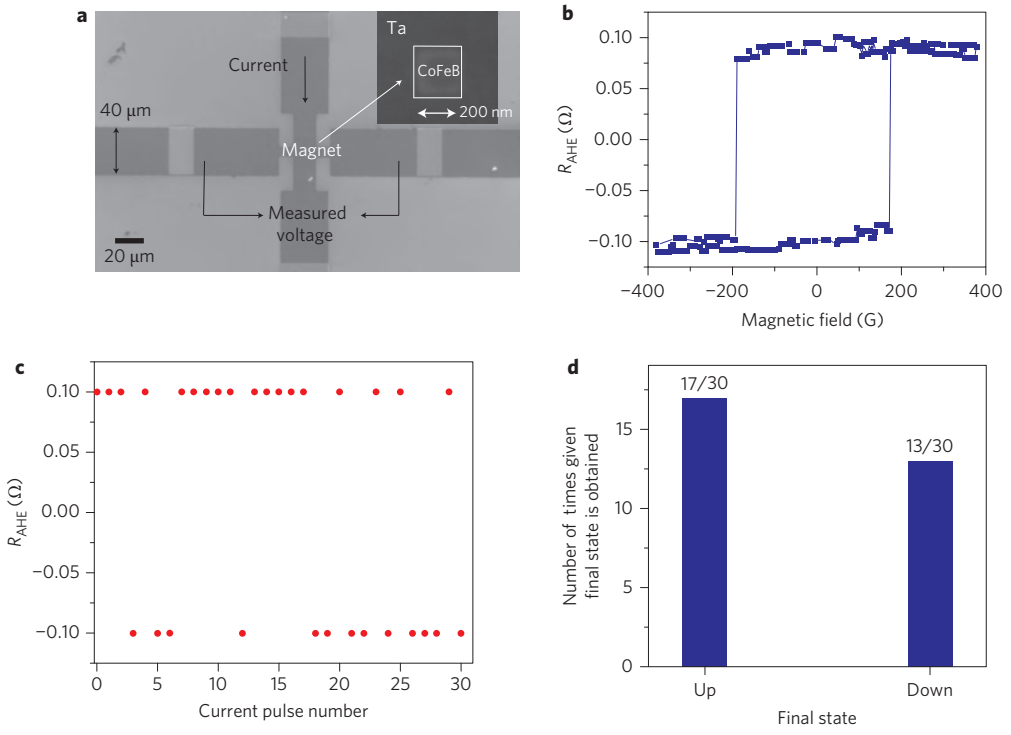

Figure 2 | Driving a perpendicularly polarized magnet to a metastable in-plane state by spin Hall effect spin torque. a, SEM images showing a Hall bar structure with a square dot (side length 200 nm) at its centre. The dot comprises Ta (10 nm)/CoFeB (1 nm)/MgO (1 nm)/Ta (~10 nm), while regions outside the dot are etched down to the bottom tantalum layer of the stack (see Methods). **b**, Anomalous Hall resistance R_{AHE} (proportional to the out-of-plane magnetization of the dot) is measured using the Hall bar structure, with a varying magnetic field applied out of plane. A square hysteresis loop is obtained, which shows that the easy axis of the magnet is out of plane. **c**, Starting with the magnet initially in the up direction, 30 successive current pulses of magnitude 1.5×10^7 A cm^{-2} are applied at 0 G. R_{AHE} is measured after every current pulse and plotted against the current pulse number. **d**, Histogram, obtained from the results of the same experiment, showing that the magnet is either up ($R_{AHE} = 0.1\ \Omega$) or down ($R_{AHE} = -0.1\ \Omega$) after a current pulse, with almost 50% probability. Accordingly, the spin Hall effect spin torque from the current pulse drives the magnet to a metastable in-plane state, from which thermal noise directs it either to the up or down state.

due to dipole coupling. Now, if the input magnet can be designed in such a way that it is not affected by the clock pulse, this will dictate the final state of the three-dot nanomagnetic chain. If the input is (↑), the chain of three dots will go to (↓↑↓), and if the input is (↓), the chain will go to (↑↓↑). Thus, the last magnet in the chain would be a function of the fixed input magnet, and information would propagate along the chain. In this Letter, we demonstrate that such a scheme is indeed possible.

We start by investigating an individual dot. All our devices were fabricated from a stack of thermally oxidized Si (substrate)/Ta (10 nm)/CoFeB (1 nm)/MgO (1 nm)/Ta (20 nm) (see Methods for details). All measurements for this work were performed at room temperature. Scanning electron microscopy (SEM) images of a typical Hall bar structure with a magnetic dot (200 nm × 200 nm) at the centre are shown in Fig. 2a. In this configuration, one can probe the magnetization by measuring the Hall resistance corresponding to the anomalous Hall effect (AHE)[26]. The anomalous Hall resistance R_{AHE} is proportional to the out-of-plane magnetization of the dot. Figure 2b presents a typical measurement. The data clearly show that the easy axis of the magnetic dot is in the out-of-plane direction. We began with a vertically up direction for the magnetization. Next, a current pulse of magnitude 1.5×10^7 A cm^{-2} was applied 30 times. The final state of the magnet was found to be up ($R_{AHE} = 0.1\ \Omega$) 17 times and down ($R_{AHE} = -0.1\ \Omega$) 13 times (Fig. 2c,d). The near 50% probability of 'up' and 'down' states demonstrates that the current flowing in the tantalum is indeed putting the magnetic dot into a metastable state from which it is driven to up or down directions by thermal noise, in accordance with the intuitive picture already presented. We have considered other possible mechanisms to explain this result, including Joule heating and the magnetic field (Oersted field) generated by current, and have concluded that these two mechanisms are not dominant factors in our experiment (Supplementary Section 8).

We next considered a system of three identical nanomagnetic dots. Figure 3a shows three fabricated dots, which are 200 nm in diameter and separated from one another by a distance of 30 nm. The dots were placed away from the cross-centre area of the Hall bars. In this configuration, the contribution to the AHE resistance from each of the dots is different, so they can be probed individually[27]. The following notation is used herein and in Fig. 3b–f to represent the magnetization states of the three adjacent magnetic dots—state of the nearest magnet, state of the middle magnet and state of the farthest magnet—where the state of each magnet can be up (↑) or down (↓). The dot nearest to the cross-centre has the maximum contribution to the AHE signal[27] (Fig. 3b). When the nearest magnet switches the change in R_{AHE} is 0.07 Ω, while for middle magnet (middle arrow) the change is 0.04 Ω and for the farthest magnet (rightmost arrow) it is 0.015 Ω (Supplementary Sections 2 and 10). If these magnets are now driven to a metastable state, they are expected to go to a mutually antiparallel state of '2 up 1 down' (↑↓↑) or '1 up 2 down' (↓↑↓) with 50% probability due to dipole coupling. To test this, a current pulse of magnitude 3×10^7 A cm^{-2} was applied at zero external magnetic field to drive the three magnets in a metastable state. Of 20 repeated measurements, the magnets proceeded to the (↑↓↑) state eight times and the (↓↑↓) state five times (Fig. 3c,d) (for details of the measurement see Supplementary Section 3). The same experiment was performed next with the three magnets

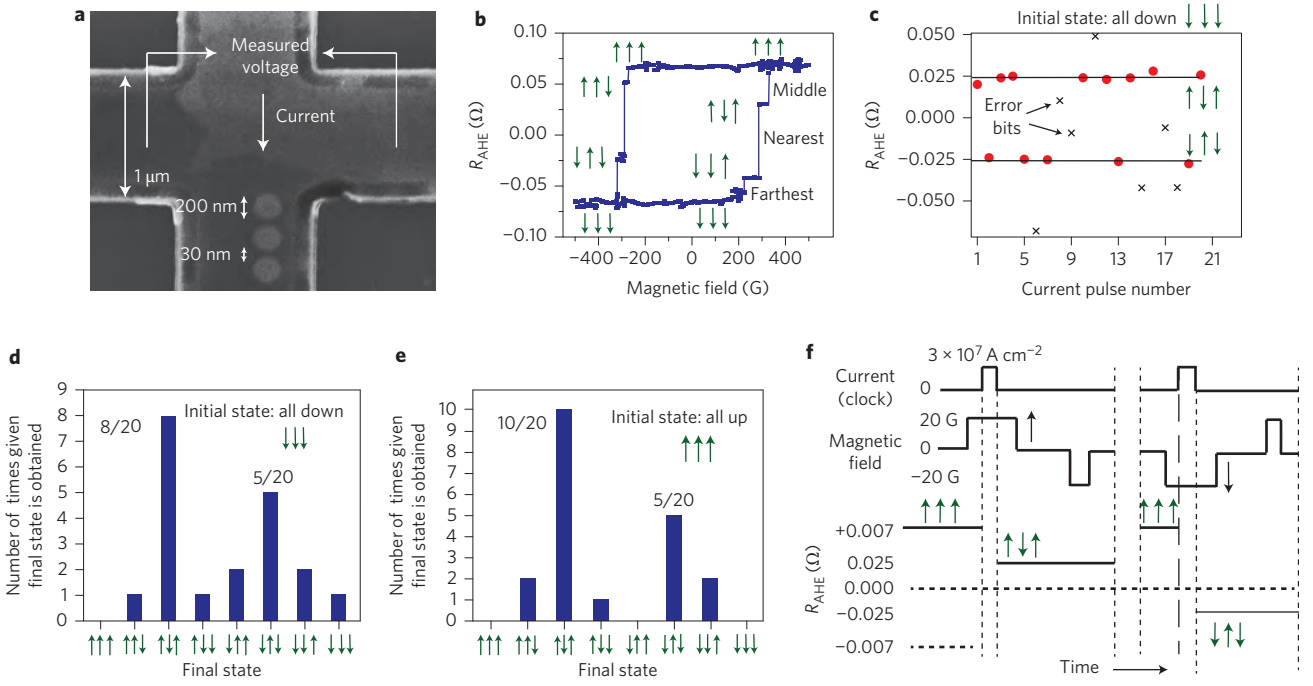

Figure 3 | Dipole coupling between adjacent magnetic dots. a, SEM image showing three circular magnetic dots of diameter 200 nm at a separation of 30 nm. **b**, Hysteresis loop (R_{AHE} versus out-of-plane magnetic field) showing three discrete jumps, each corresponding to one magnet switching between up and down. Green arrows: direction of magnetization of each dot. The dot farthest from the cross-centre (rightmost arrow in each set of three arrows) has the lowest contribution to R_{AHE}, whereas the one that is closest (leftmost arrow in each set of three arrows) has the highest contribution[27]. **c**, Starting with all three magnets initially down, a current pulse of magnitude 3×10^7 A cm^{-2} is applied 20 times at a field of 0 G. The R_{AHE} of the final state after each current pulse is plotted against current pulse number. Bold lines are drawn through the expected final states, '2 up 1 down' (↑↓↑) and '2 down 1 up' (↓↑↓), which we obtain 13 out of 20 times. The other seven times indicate states where adjacent magnets are parallel to each other. These are the error bits, represented by crosses. **d**, Histogram, obtained from the results of the same experiment, showing the dominance of mutually antiparallel aligned states: (↑↓↑) eight times and (↓↑↓) five times. This is a result of dipole coupling between adjacent dots making these two states the lowest-energy configuration. **e**, When the same experiment is repeated with all magnets initially up, the (↑↓↑) state is formed ten times and the (↓↑↓) state five times. **f**, When the same current pulse is instead applied in the presence of a 20 G field, with the magnets initially all in the up state, they always go to the (↑↓↑) state. Similarly at −20 G, the current pulses drive them to the (↓↑↓) state. Thus, the bias magnetic field controls the final state of the magnets. Either of the states (↑↓↑) and (↓↑↓) is stable unless another large current pulse or a magnetic field (higher than the coercivity of the dots, ~300 G), is applied.

initially in the upward direction. Of 20 trials, on ten occasions the final state was (↑↓↑) and on five occasions (↓↑↓) (Fig. 3e). The slight deviation from 50% probability may be due to the small sample size (in terms of number of repetitions) and also due to errors that could arise in dipole coupling, which has been extensively studied[28].

The same experiment was repeated, but in the presence of a bias magnetic field. When the current pulse was applied with a 20 G field along the up direction, the magnets always went to the '2 up 1 down' state (↑↓↑). Similarly, when the current pulse was applied at −20 G, the magnets always went to the '2 down 1 up' state (↓↑↓) (Fig. 3f, Supplementary Fig. 4a,b). Thus, the external magnetic field breaks the symmetry of the system and causes the magnets to prefer one configuration over the other, depending on the polarity of the magnetic field. The fact that the current in tantalum can drive the three-dot chain into a metastable state from which a magnetic field input can deterministically drive it to one of two dipole-coupled states clearly demonstrates that the spin Hall current can be used as an efficient clocking scheme for nanomagnetic logic.

As a demonstration of a complete system, we next fabricated a three-dot chain of nanomagnets (500 nm × 500 nm) together with an input magnet. The dots were spaced by 30 nm. The input magnet was large (a few micrometres on each side) and ~30 nm away from the first magnet in the three-dot chain (Fig. 4a). In the AHE measurement, a larger change in R_{AHE} at smaller switching field corresponds to the switching of the large input magnet, while smaller jumps at a higher switching field (Fig. 4b) must arise from the smaller magnetic dots, because the switching field reduces with increasing size of the dots (Supplementary Section 5). This allows us to probe the input magnet and the three-dot chain separately. To prepare the input state, we applied a current pulse in the presence of a 20 G magnetic field in the up direction (Supplementary Section 6). This put the large input magnet in the up direction, which acted as an input to the chain. From Fig. 3e, this condition should drive the three-dot chain to the '2 up 1 down' state (↑↓↑). On the other hand, if the input is strong, then the up state of the input magnet should drive the three-dot chain to a '2 down 1 up state' (↓↑↓). To test this, we started with all magnets in the upward direction. Application of the clocking current pulse in the presence of a 20 G field then caused the input magnet to remain upward while the other three magnets proceeded to the '2 down 1 up' configuration (Fig. 4c). Similarly, application of a current pulse at −20 G with all magnets initially down resulted in the input dot remaining down and the other dots going to the '2 up 1 down' configuration (for details of the measurement see Supplementary Section 7). We repeated the experiment five times each for the input magnet up and down and observed the same result (Fig. 4d,e). It is important to note that the 20 G magnetic field has only been used to prepare the input state and is not fundamentally necessary for the operation of the logic scheme. In a practical implementation, the input magnet will be the output of a previous stage and can be electrically isolated from the magnetic chain so that the clock current does not flow through it.

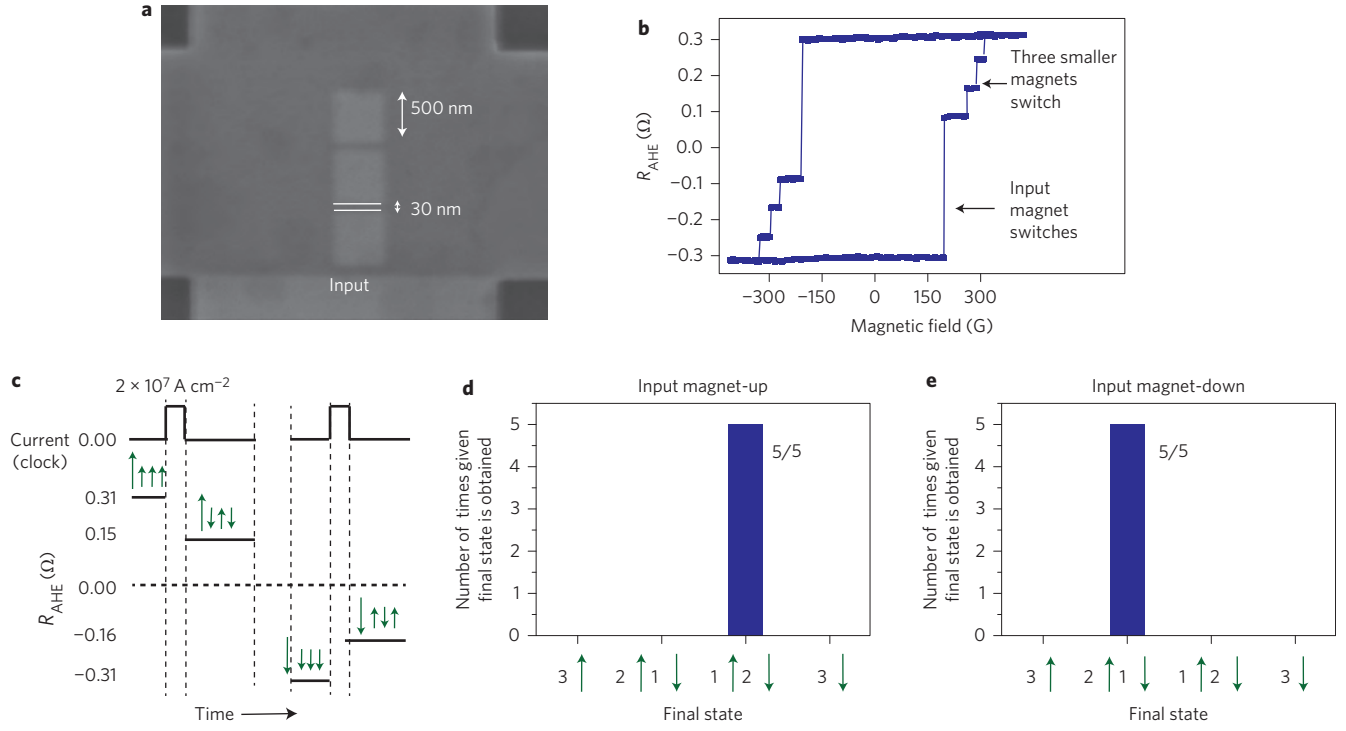

Figure 4 | Information propagation along a chain of magnetic dots. a, SEM image showing three square magnetic dots of side length 500 nm at a separation of 30 nm, next to a larger dot (each side a few micrometres in length). This large magnet acts as the fixed input bit. **b**, R_{AHE} measurement of the device shows two different types of jump: a larger change in R_{AHE} (0.4 Ω) corresponding to the bigger input dot and three smaller jumps (0.08 Ω each) corresponding to the three smaller dots. **c**, A current pulse of magnitude 2×10^7 A cm^{-2} is applied at 20 G on the device with all magnets initially up. The input magnet (magnetization direction indicated by the big green arrow) remains up while the other magnets (small green arrows) go to the '2 down 1 up' state, thus following the input magnet. When a current pulse is applied at −20 G with all magnets initially down, the input magnet remains down and the other magnets go to the '2 up 1 down' state. **d**,**e**, Histograms, obtained from multiple runs of the same experiment (Fig. 4c), showing that the '2 down 1 up' state is always achieved when the input magnet is up and the '2 up 1 down' state when the input magnet is down. Thus, the magnetization state of the input magnet controls the final state of the other magnets.

The current amplitude needed for our experimental demonstration of clocking was ~2 mA with a tantalum wire of width 1 μm and thickness 10 nm. This is significantly lower (more than 100 times lower) than the current needed (760 mA) in the only on-chip demonstration[11] of magnetic field-based clocking for a much smaller magnet (60 nm × 90 nm). The current needed in our scheme scales linearly with the width of the magnet, making the clocking scheme scalable. More importantly, the current needed to clock the magnet scales with the thickness of the tantalum. In an optimized structure for a 60 nm × 90 nm magnet where the width of the tantalum wire is the same as the magnet, the current amplitude could be reduced to 120 μA. The current amplitude can be further decreased by reducing the thickness of the wire[22]. Even with idealistic approximations for magnetic field clocking, the current needed in spin Hall clocking can be projected to be roughly 100 times lower than magnetic field clocking (for discussion see Supplementary Section 9).

Notably, in nanomagnetic logic, the dominant mechanism for energy dissipation is Joule heating (I^2R loss). Much of the resistance R arises from the long interconnects that bring the clock signal to the magnets. Most parts of these interconnects could be made of a low resistivity metal such as copper. The higher-resistivity tantalum necessary to generate the spin Hall effect could be restricted to being used only under the magnet and a few tens of nanometres on either side of it. Thus, when going from conventional field-clocked to spin Hall current-clocked nonmagnetic logic, there should only be, at most, a several-fold increase in resistance. On the other hand, there is a more than four-order-of-magnitude reduction in I^2. Therefore, overall, a reduction in energy dissipation of three to four orders of magnitude is expected for the demonstrated scheme compared with conventional nanomagnetic logic. We have estimated the overall energy dissipation in our scheme following the methodology proposed by Nikonov and colleagues[29]. This methodology takes into account not only the intrinsic device but also the external circuitry. Because the logic architecture in our scheme is similar to that in conventional nanomagnetic logic, we could directly use the same assumptions made for the driving circuitry for nanomagnetic logic, as in ref. 29. The calculation needs one to assume a feature size, a pulsewidth for the clock signal, the current amplitude and the resistivity of the wire. The last two can be taken directly from our experiment, and the first two need to be estimated. Supplementary Section 11 provides details of the assumptions made for the calculation, and their rationale, as well as comparative charts. Compared with the results published in ref. 29, such a reduction in energy dissipation could make the demonstrated scheme comparable to CMOS circuits. Importantly, the reduction in current and thus energy dissipation could be further lowered by using other metals that have demonstrated larger spin Hall angles, such as CuBi[30].

To summarize, we have demonstrated that a chain of nanomagnets can be clocked by a charge current using the spin Hall effect in such a way that an input magnet can dictate how the signal propagates through the magnetic chain. Each magnet acts as one inverter, and the magnetic chain acts as a set of three cascaded inverters. The architecture needed to implement logic using this scheme is identical to that used in conventional field-clocked nanomagnetic logic, but where the field generating the clocking lines is replaced by spin Hall metal. However, the fact that no magnetic field is

needed significantly reduces energy dissipation in the clocking, which has previously proved to be a fundamental bottleneck in nanomagnetic logic schemes. For robust implementation, design solutions will have to be found to reduce the error probability associated with dipole coupling to acceptable limits[28].

Methods

The stack comprising thermally oxidized Si substrate/Ta (10 nm)/CoFeB (1 nm)/MgO (1 nm)/Ta (20 nm) was first processed into Hall bars by photolithography and argon ion milling. The Hall bars contained the entire thin-film stack, with the region outside the Hall bars etched down to the insulating Si substrate. A dot pattern of 8-nm-thick titanium, which acts as an etching mask, was fabricated on the Hall bar by electron-beam lithography. Argon ion milling was also used to etch the stack in the region outside the dot patterns, down to the bottom tantalum layer. The dots therefore comprised Ta (10 nm)/CoFeB (1 nm)/MgO (1 nm)/Ta ($\sim$ 10 nm), and the regions of the Hall bar outside the dots were etched down to the bottom tantalum layer.

For anomalous Hall resistance measurement, current was applied using a d.c. and a.c. current source and the Hall voltage was measured using a nanovoltmeter in the usual way. The same current source was used to apply current pulses for clocking. A unipolar current pulse with a duration of 1 s was used for all measurements. The polarity of the current pulse was positive for all data unless explicitly stated otherwise. A negative current pulse has the same effect as a positive current pulse of the same magnitude for clocking experiments, because the magnet will be driven to its metastable in-plane state from its out-of-plane direction by both positive and negative current pulses (Supplementary Fig. 1c), and there is no in-plane magnetic field present to cause deterministic switching. Only in Supplementary Figs 1e,f and 8b–e were both positive and negative current pulses applied, and the magnetization switching was determined by the polarity of the current pulse. All measurements were carried out at room temperature.

Received 3 September 2013; accepted 16 October 2013; published online 17 November 2013

References

1. Salahuddin, S. & Datta, S. Interacting systems for self-correcting low power switching. *Appl. Phys. Lett.* **90,** 093503 (2007).
2. Behin-Aein, B., Datta, D., Salahuddin, S. & Datta, S. Proposal for an all-spin logic device with built-in memory. *Nature Nanotech.* **5,** 266–270 (2010).
3. Bandyopadhyay, S. & Cahay, M. *Introduction to Spintronics* (CRC, 2008).
4. Nikonov, D. E., Bourianoff G. I. & Ghani, T. Proposal of a spin torque majority gate logic. *IEEE Electron. Dev. Lett.* **32,** 1128–1130 (2011).
5. Ikeda, S. *et al.* Magnetic tunnel junctions for spintronic memories and beyond. *IEEE Trans. Electron. Dev.* **54,** 991–1002 (2007).
6. Ohno, H., Endoh, T., Hanyu, T., Naoki, K. & Ikeda, S. Magnetic tunnel junction for nonvolatile CMOS logic. *IEEE IEDM Tech. Digest* **2010,** 218–221 (2010).
7. Cowburn, R. P. & Welland, M. E. Room temperature magnetic quantum cellular automata. *Science* **287,** 1466–1468 (2000).
8. Imre, A. *et al.* Majority logic gate for magnetic quantum-dot cellular automata. *Science* **311,** 205–208 (2006).
9. Atulasimha, J. & Bandyopadhyay, S. Bennett clocking of nanomagnetic logic using multiferroic single-domain nanomagnets. *Appl. Phys. Lett.* **97,** 173105 (2010).
10. Carlton, D. B., Emley, N. C., Tuchfeld, E. & Bokor, J. Simulation studies of nanomagnet-based logic architecture. *Nano Lett.* **8,** 4173–4178 (2008).
11. Alam, M. T. *et al.* On-chip clocking of nanomagnetic logic lines and gates. *IEEE Trans. Nanotechnol.* **11,** 273–286 (2012).
12. Ju, X. *et al.* Nanomagnetic logic from partially irradiated Co/Pt nanomagnets. *IEEE Trans. Nanotechnol.* **11,** 97–104 (2012).
13. Breitkreutz, S. *et al.* Majority gate for nanomagnetic logic with perpendicular magnetic anisotropy. *IEEE Trans. Magn.* **48,** 4336–4339 (2012).
14. Lambson, B., Carlton, D. & Bokor, J. Exploring the thermodynamic limits of computation in intergrated systems: magnetic memory, nanomagnetic logic, and the Landauer limit. *Phys. Rev. Lett.* **107,** 010604 (2011).
15. Roy, K., Bandyopadhyay, S. & Atulasimha, J. Hybrid spintronics and straintronics: a magnetic technology for ultra low power energy computing and signal processing. *Appl. Phys. Lett.* **99,** 063108 (2011).
16. Liu, L. *et al.* Spin–torque switching with the giant spin Hall effect of tantalum. *Science* **336,** 555–558 (2012).
17. Liu, L., Lee, O. J., Gudmundsen, T. J., Ralph, D. C. & Buhrman, R. A. Current-induced switching of perpendicularly magnetized magnetic layers using spin torque from the spin Hall effect. *Phys. Rev. Lett.* **109,** 096602 (2012).
18. Haazen, P. P. J. *et al.* Domain wall depinning governed by the spin Hall effect. *Nature Mater.* **12,** 299–303 (2013).
19. Miron, I. M. *et al.* Current-driven spin torque induced by the Rashba effect in a ferromagnetic metal layer. *Nature Mater.* **9,** 230–234 (2010).
20. Miron, I. M. *et al.* Perpendicular switching of a single ferromagnetic layer induced by in-plane current injection. *Nature* **476,** 189–193 (2011).
21. Suzuki, T. *et al.* Current-induced effective field in perpendicularly magnetized Ta/CoFeB/MgO wire. *Appl. Phys. Lett.* **98,** 142505 (2011).
22. Kim, J. *et al.* Layer thickness dependence of the current induced effective field vector in Ta/CoFeB/MgO. *Nature Mater.* **12,** 240–245 (2013).
23. Hirsch, J. E. Spin Hall effect. *Phys. Rev. Lett.* **83,** 1834–1837 (1999).
24. Ikeda, S. *et al.* A perpendicular anisotropy CoFeB–MgO magnetic tunnel junction. *Nature Mater.* **9,** 721–724 (2010).
25. Bhowmik, D., You, L. & Salahuddin, S. Possible route to low current, high speed, dynamic switching in a perpendicular anisotropy CoFeB–MgO junction using spin Hall effect of Ta. *IEEE IEDM Tech. Digest* **2012,** 29.7.1–29.7.4 (2012).
26. Nagaosa, N., Sinova, J., Onoda, S., MacDonald, A. H. & Ong, N. P. Anomalous Hall effect. *Rev. Mod. Phys.* **82,** 1539–1592 (2010).
27. Alexandrou, M. *et al.* Spatial sensitivity mapping of Hall crosses using patterned magnetic nanostructures. *J. Appl. Phys.* **108,** 043920 (2010).
28. Carlton, D. B. *et al.* Investigation of defects and errors in nanomagnetic logic circuits. *IEEE Trans. Nanotechnol.* **11,** 760–762 (2012).
29. Nikonov, D. E. & Young, I. Overview of beyond-CMOS devices and a uniform methodology for their benchmarking. *Proc. IEEE* http://dx.doi.org/10.1109/JPROC.2013.2252317 (2013).
30. Niimi, Y. *et. al.* Giant spin Hall effect induced by skew scattering from bismuth impurities inside thin film CuBi alloys. *Phys. Rev. Lett.* **109,** 156602 (2012).

Acknowledgements

The authors thank E. Chen and X. Tang of Grandis Corporation for help with material preparation, and D. Nikonov and J. Bokor for valuable discussions. This work was supported in part by the Defense Advance Research Projects Agency Non-Volatile Logic Program, the National Science Foundation Center for Energy Efficient Electronics Science Centre at Berkeley, and the Semiconductor Research Corporation Western Institute of Nanoelectronics centre.

Author contributions

L.Y. fabricated the devices. D.B. and L.Y. performed measurements. S.S. conceived and supervised the overall project. All authors discussed and analysed data and participated in writing the manuscript.

Additional information

Supplementary information is available in the online version of the paper. Reprints and permissions information is available online at www.nature.com/reprints. Correspondence and requests for materials should be addressed to S.S.

Competing financial interests

The authors declare no competing financial interests.